International Journal of Control, Automation and Systems 14(4) (2016) 1064-1073
http://dx.doi.org/10.1007/s12555-014-0395-7
ISSN:1598-6446 eISSN:2005-4092
http://www.springer.com/12555

Minimizing Human-exoskeleton Interaction Force by Using Global Fast Sliding Mode Control

Duong Mien Ka*, Cheng Hong, Tran Huu Toan, and Jing Qiu

Abstract: A critical issue in the model-based control of performance-augmenting exoskeleton systems is the unknown nonlinear dynamic properties of the systems or the uncertainties. An improper estimation of the system dynamics can cause instabilities in the system and generate considerable human-exoskeleton interaction forces during human motions. Thus, the controller of such exoskeleton systems needs to add robustness to stabilize it against the uncertainties. In this paper, we propose a global fast sliding mode control algorithm integrated in a hybrid controller for each exoskeleton leg to minimize human-exoskeleton interaction forces. By doing so, the proposed algorithm does not require an exact estimation of the dynamic properties of the exoskeleton system, but still minimizes the physical human-exoskeleton interaction (pHEI) forces. Finally, the performance of the proposed algorithm is verified by experiments on our lower exoskeleton system, which is used for human power augmentation and called "PRMI" exoskeleton. Our experimental results show that the proposed control algorithm provides a good control quality for the PRMI exoskeleton. The PRMI exoskeleton can support a wearer carrying heavy load while tracking the rapid movements of the wearer without obstructing them.

Keywords: Exoskeleton, human-exoskeleton interaction, performance-augmenting exoskeleton, sliding mode control.

1. INTRODUCTION

An exoskeleton system is defined as an electromechanical structure worn by a user, and matches the shape and functions of the human body [1]. Exoskeletons have been studied since the late 1960s and were classified according to different applications. Almost all recent researches have concentrated on making walking aid systems for gait disorder persons, called rehabilitation active exoskeleton [2–11]. These exoskeletons belong to active exoskeletons. They impose significant interaction forces on the wearer and assist the wearer during walking. In contrast, passive exoskeletons, called performance augmenting exoskeletons, were designed with the aim of providing most of the strength necessary for walking or carrying heavy loads in an able-bodied user. The goal of these systems is that the interaction forces should be very small so that the wearer can walk easily [12–17].

For a performance-augmenting exoskeleton, one of the major challenges is to control the exoskeleton track wearer's movements rapidly and comfortably, without obstructing the wearer. In other words, the human-exoskeleton interaction forces must be very small. In order to solve this issue, model-based control algorithms were used in the literature. Kazerooni *et al*. developed a sensitivity amplification control algorithm for their exoskeleton system, called BLEEX [18–20]. The BLEEX system increases the system's closed loop sensitivity to its wearer's forces and torques without any measurement from the wearer in its control module [20]. However, this control algorithm relies on the dynamic model of the system without dynamic uncertainty compensation. In order to decrease the dependence on the dynamic model, Kazerooni *et al*. divided the entire system into a swing leg model and a stance leg model. Then they used a hybrid control algorithm including a position controller for the stance leg and a sensitivity amplification controller for the swing leg [21]. Unfortunately, this approach still relied on the accuracy of the estimated system dynamic model. Yang *et al*. developed a control algorithm using neural networks [22] to estimate the inverse dynamic model of their exoskeleton system. However, it is difficult to apply

Manuscript received October 1, 2014; revised May 28, 2015 and August 2, 2015; accepted September 10, 2015. Recommended by Associate Editor Sukho Park under the direction of Editor PooGyeon Park. This research was supported by the grant of National Natural Science Foundation of China (Grant No. 61273256). The authors would like to thank the associate editor and the reviewers for their valuable comments.

Duong Mien Ka and Tran Huu Toan are with the School of Automation Engineering, University of Electronic Science and Technology of China and the Faculty of Electronics, Industrial University of Ho Chi Minh City, Vietnam (e-mails: {duongmienka, huutoancdt}@gmail.com). Cheng Hong and Jing Qiu are with the School of Automation Engineering, University of Electronic Science and Technology of China, China (e-mails: hchenguestc@gmail.com, qiujing@uestc.edu.cn).
* Corresponding author.

practically due to the computational complexity. Then, Yang *et al*. used an inverse dynamic-based control algorithm that included compensation for uncertainty dynamic error by RBF networks as their enhanced control algorithm [23]. Similar to the impedance control algorithm for exoskeleton systems, this method required complicated force sensors installed in the human-exoskeleton interaction positions to measure the interaction forces. In this case, it was difficult to measure the reliable interaction forces due to unstable sensor locations. This approach also increased the complexity of the system.

At Nanyang Technological University, Low *et al*. developed a lower extremity exoskeleton for load carrying, called LEE [24]. To collect the joint information of the pilot, they used an inner exoskeleton that was attached to the pilot and an outer exoskeleton that supported the load carrying for the pilot. However, this configuration made the system more complicated and made the pilot feel uncomfortable during walking.

Another exoskeleton system targeting disabled patients in hospitals, called HAL (Hybrid Assistive Limb), was developed by Sankai *et al*. [25]. However, HAL was also used to support workers with physically demanding jobs such as disaster rescue or construction. This exoskeleton used myoelectricity (EMG) signals as primary command signals and performed according to user's intentions based on EMG signals. The EMG-based controller has major disadvantages in that the user senses discomfort during walking and the accuracy of EMG electrode sensors is affected if the system is used by different users. It is not stable to operate in complicated environments related to rescue or military.

To solve the above issues, sliding mode control appoaches can be used to design robust controllers in complex dynamic systems. In addition, the PRMI exoskeleton is a complex system operating under uncertainty conditions. Therefore, sliding mode control can eliminate any discrepancy between the real system and its estimation model [26]. However, the PRMI exoskeleton requires tracking the wearer rapidly without obstructing. The normal sliding mode control may not solve this requirement because its asymptotical convergence of system states is overcome. So, in this paper, we propose an advanced sliding mode control called the global fast terminal sliding mode control (GFSMC) [27].

Fast terminal sliding mode control can make the system states converge to zero in a finite time. The convergent charactersistic of fast terminal sliding mode control is superior to that of the normal sliding mode control. Moreover, there is no switch function in terminal sliding mode control; therefore, the chattering phenomenon is evitable. In this paper, GFSMC is integrated in a hybrid controller. By doing so, the proposed controller becomes capable of coping with the unknown dynamic uncertainties and makes the swing leg track the human's performances rapidly. In addition, the exoskeleton system avoids using the complicated force sensors installed at the human-exoskeleton interaction positions.

The proposed control algorithm was verified on our PRMI lower exoskeleton system. The PRMI exoskeleton consists of two subsystems: The first is the swing leg model controlled by a global fast sliding mode controller in order to increase the stability of the system. The second is the stance leg model controlled by a proportional-derivative (PD) controller including gravity compensation. Experimental results show that the proposed control algorithm can provide good control quality for the PRMI exoskeleton system without an exact estimation of dynamic uncertainties. The exoskeleton moved in concert with the wearer while supporting heavy load carrying with very small interaction forces.

The rest of this paper is organized as follows: Section 2 describes the dynamic models and the physical human-exoskeleton interaction (pHEI). Section 3 introduces the proposed control algorithm, including a PD controller and a global fast sliding mode controller. Section 4 presents the PRMI exoskeleton used in the experiments. Experiments and analysis are introduced in Section 5. Finally, conclusions and future works are discussed in Section 6.

2. DYNAMIC MODELING AND PHYSICAL HUMAN EXOSKELETON INTERACTION MODEL

The investigation of the dynamic characteristics of a multi-DOF exoskeleton system in walking space is very complicated. The abduction-adduction motions can be considered as quasi-static maneuvers with little dynamical effect on the rest of the system [21]. For simplicity, the dynamic characteristics of the abduction-adduction motions in the frontal plane are ignored. Thus, the investigation of the dynamic characteristics is implemented only in the sagittal plane as in Fig. 1. The entire PRMI exoskeleton is separated into two subsystems that consist of a stance leg model and a swing leg model. The swing leg undergoes larger motion, but it only supports its own weight [20]. The swing leg in the sagittal plane is expressed by a 3-DOF series of links (white serial links in Fig. 1). The stance leg goes through a small motion, but supports the entire torso and payload. Hence, it needs larger torque. The stance leg in the sagittal plane is expressed by a 4-DOF series of links (gray links in Fig. 1).

2.1. Stance leg model

Stance leg is the leg that is on the ground and supports the entire body weight as illustrated in Fig. 1. The dynamic equation of the stance leg model can be written in the general form as follows (the subscript "st" indicates

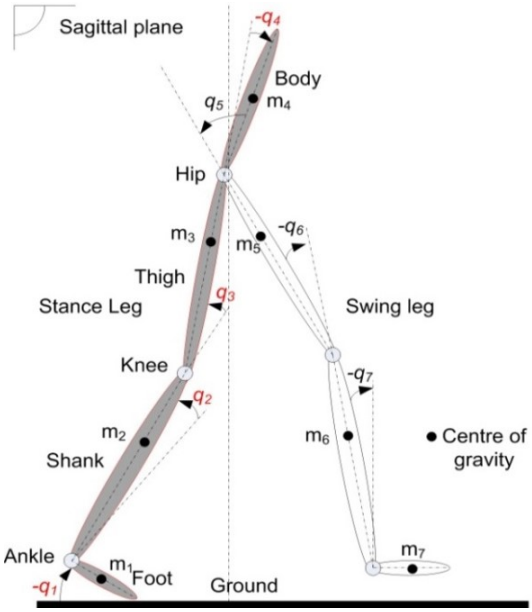

Fig. 1. Stance leg model (gray links) and swing leg model (white links).

the stance leg):

$$M_{st}(q_e)\ddot{q}_e + C_{st}(q_e,\dot{q}_e)\dot{q}_e + G_{st}(q_e) = T_{act} + T_{int}, \quad (1)$$

where $q_e = [q_1, q_2, q_3, q_4]^T \in R^{4\times1}$ is a vector of exoskeleton's joint angular positions; $T_{act} = [T_1, T_2, T_3, T_4]^T \in R^{4\times1}$ is a vector of actuator joint torques; $M_{st}(q_e) \in R^{4\times4}$ is a symmetric positive-definite inertia matrix; $C_{st}(q_e,\dot{q}_e) \in R^{4\times4}$ is a centripetal and Coriolis matrix; $G_{st}(q_e) \in R^{4\times1}$ is a vector of gravitational torques. At toe and ankle joints T_1 and T_2 are equal to zero because the two DOFs are not actuated but controlled by the wearer; $T_{int} \in R^{4\times1}$ is a vector of joint interaction torques imposed by the wearer.

2.2. Swing leg model

Swing leg is the leg that has no interaction with the ground and swings the leg forward as shown in Fig. 1. Using Lagrange formulation, the dynamic equation of the swing leg model is derived as follows (the subscript "sw" indicates the swing leg):

$$M_{sw}(q_e)\ddot{q}_e + C_{sw}(q_e,\dot{q}_e)\dot{q}_e + G_{sw}(q_e) = T_{act} + T_{int}, \quad (2)$$

where $q_e = [q_5, q_6, q_7]^T \in R^{3\times1}$ is a vector of exoskeleton's joint angular positions; $T_{act} = [T_5, T_6, T_7]^T \in R^{3\times1}$ is a vector of actuator joint torques; $M_{sw}(q_e) \in R^{3\times3}$ is a symmetric positive-definite inertia matrix; $C_{sw}(q_e,\dot{q}_e) \in R^{3\times3}$ is a centripetal and Coriolis matrix; $G_{sw}(q_e) \in R^{3\times1}$ is a vector of gravitational torques. T_7 is equal to zero because the degree of freedom is not actuated but controlled by the wearer. $T_{int} \in R^{3\times1}$ is a vector of joint interaction torques imposed by the wearer. Refer Appendix section for more details of M, C, G of the stance and swing legs.

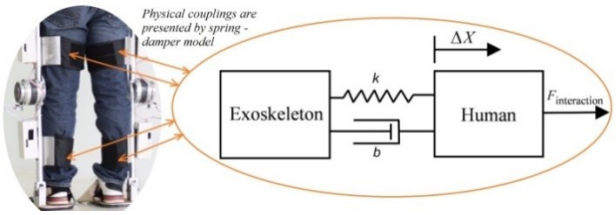

Fig. 2. Physical human-exoskeleton interaction model.

In the absence of friction and gravity, from (1) and (2), the interaction torques for the swing leg model as well as the stance leg model can be written in general as follows:

$$T_{int} = M(q_e)\ddot{q}_e + C(q_e,\dot{q}_e)\dot{q}_e + G(q_e) - T_{act}. \quad (3)$$

2.3. Physical human-exoskeleton interaction model (pHEI)

The design of the PRMI exoskeleton was chosen as a pseudo-anthropomorphic design. The exoskeleton has leather bands as physical couplings in the middle of the thigh and shank segments that help the wearer to wear the exoskeleton. Any motion of the exoskeleton occurs in contact with a human and any interaction force is exerted by the exoskeleton on the wearer through these physical connection points. A spring-damper model was used in this study to express the interaction forces (see Fig. 2). This model acts as a physical human-exoskeleton interaction model that was verified in the literature [21].

During walking, the wearer creates interaction torques that impose on the exoskeleton due to the deviation between the human's joint angular position (q_h) and that of the exoskeleton (q_e). If the exoskeleton is able to track the wearer's voluntary motion quickly and simultaneously, the deviation between q_h and q_e is very small. Hence, the interaction torques tend to zero. In other words, the wearer moves together comfortably with the exoskeleton. Consequently, the interaction model presents an interaction torque as a function of $(q_h, \dot{q}_h, \ddot{q}_h, q_e, \dot{q}_e, \ddot{q}_e)$. For many exoskeleton researches in recent years, a combination of nonlinear elastic and viscoelastic elements was used as a compliant connection. The interaction torque can be expressed as follows:

$$T_{int} = k(q_h - q_e) + b(\dot{q}_h - \dot{q}_e), \quad (4)$$

where k and b are matrices of stiffness and damping coefficients of the interaction model, respectively. T_{int} is a vector of joint interaction torques imposing on the exoskeleton.

3. THE PROPOSED HYBRID CONTROL ALGORITHM

For exoskeleton robots, human-exoskeleton interaction (HEI) usually exists during human movements and it

should be considered in exoskeleton control. HEI includes a cognitive human-exoskeleton interaction model (cHEI) and a physical human-exoskeleton interaction model (pHEI) as in Fig. 3. The role of the cHEI is to make the exoskeleton recognize the human's intention such as phase transition, etc. In the PRMI exoskeleton, cHEI performs as a phase selector to recognize the next phase while pHEI implies the physical coupling between the exoskeleton and the wearer (see Section 2). According to the discussion in the previous section, the desired interaction torques imposing on the wearer should tend to zero during movements. Therefore, the proposed control strategy must ensure that the interaction torques tend to zero. The basic control approaches to the management of the pHEI can be classified into two groups: feed-forward control and feedback control. Feed-forward systems execute control action using a model-based estimation.

In this paper, the hybrid control algorithm is applied to the lower exoskeleton, the PD control algorithm to the stance leg and the global fast sliding mode control to the swing leg. Actually, enhanced control algorithms can also be applied to the stance leg. However, according to the previous analysis, though the stance leg has a small range of operation, it needs larger required torques while the swing leg has a larger range of motion but needs smaller required torques. Hence, joint angular position tracking is not as important in the stance leg as in the swing leg. We apply the PD control algorithm to the stance leg and the global fast sliding mode control to the swing leg in the second version of the PRMI exoskeleton system.

3.1. Stance leg: PD controller

In the control scheme, the interaction model and gravity compensation blocks are included as in Fig. 4. We design the PD controller including a gravity compensator for the stance leg phase as follows:

$$T_{act} = K_p\left(q_h - q_e\right) + K_d\left(\dot{q}_h - \dot{q}_e\right) + \hat{G}_{st}\left(q_e\right), \tag{5}$$

where q_h, q_e are vectors of joint angular positions of the wearer and the exoskeleton limbs, respectively; $\hat{G}_{st}(q_e)$ is vector of estimated torques due to gravity; T_{act} is a vector of joint actuator torques. Substituting (5) and (4) into (1), we get the closed-loop system as follows:

$$\begin{aligned} M_{st}\left(q_e\right)\ddot{q}_e + C_{st}\left(q_e,\dot{q}_e\right)\dot{q}_e =& (K_p + k)\tilde{q} + (K_d + b)\dot{\tilde{q}} \\ &+ \triangle G_{st}\left(q_e\right), \end{aligned} \tag{6}$$

where $\tilde{q} = q_h - q_e$; $\dot{\tilde{q}} = \dot{q}_h - \dot{q}_e$; $\triangle G_{st}(q_e) = \hat{G}_{st}(q_e) - G_{st}(q_e)$ is the gravity estimation error. We assume that the gravity estimation error is very small (i.e., $\triangle G_{st}(q_e) \approx 0$) and we set

$$\begin{cases} K_P = K_p + k, \\ K_D = K_d + b, \\ u = M_{st}\left(q_e\right)\ddot{q}_h + C_{st}\left(q_e,\dot{q}_e\right)\dot{q}_h. \end{cases}$$

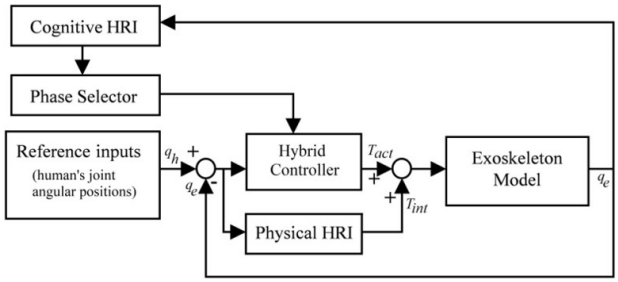

Fig. 3. Hybrid control scheme of the PRMI exoskeleton system.

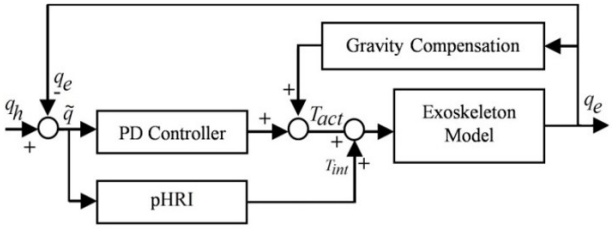

Fig. 4. PD control diagram (Stance leg).

Then (6) is rewritten as follows:

$$M_{st}\left(q_e\right)\ddot{\tilde{q}} + \left(C_{st}\left(q_e,\dot{q}_e\right) + K_D\right)\dot{\tilde{q}} + K_P\tilde{q} = u. \tag{7}$$

Defining the Lyapunov function

$$V = \frac{1}{2}\dot{\tilde{q}}^T M_{st}\dot{\tilde{q}} + \frac{1}{2}\tilde{q}^T K_P\tilde{q}, \tag{8}$$

where M_{st} and K_P are positive definite matrices, V is global positive definite.

$$\begin{aligned} \dot{V} &= \dot{\tilde{q}}^T M_{st}\ddot{\tilde{q}} + \frac{1}{2}\dot{\tilde{q}}^T\dot{M}_{st}\dot{\tilde{q}} + \dot{\tilde{q}}^T K_P\tilde{q}, \\ &= \dot{\tilde{q}}^T\left(M_{st}\ddot{\tilde{q}} + \frac{1}{2}\dot{M}_{st}\dot{\tilde{q}} + K_P\tilde{q}\right). \end{aligned} \tag{9}$$

Using the characteristic of $\dot{M}_{st}\left(q_e\right) = 2C_{st}\left(q_e,\dot{q}_e\right)$ we have

$$\dot{V} = \dot{\tilde{q}}^T\left(M_{st}\ddot{\tilde{q}} + C_{st}\dot{\tilde{q}} + K_P\tilde{q}\right) = -\dot{\tilde{q}}^T\left(K_D + C_{st}\right)\dot{\tilde{q}} \tag{10}$$

with $\|C_{st}\left(q_e,\dot{q}_e\right)\| \le \|\mu_0\|$, μ_0 is known, K_D can be chosen so that $K_D + C_{st}$ is positive definite. According to Lyapunov criterion, the system (7) is stable when $t \to \infty$. That means $\tilde{q} \to \infty$ or $q_e \to q_h$, $T_{int} \to 0$; thus, the exoskeleton shadows the wearer's movements quickly with a very small effort.

3.2. Swing leg: global fast sliding mode controller

The swing leg controller is designed according to the model-based control algorithm that relies on the precision of the estimated model. However, it is difficult to estimate the dynamic characteristics of real systems exactly due to unknown uncertainties. In such cases, the sliding mode

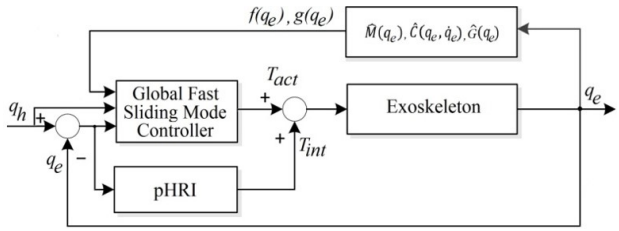

Fig. 5. Global fast sliding mode controller (Swing leg).

control approaches have proven to be one of the efficient tools used to design robust controllers for complex nonlinear systems with uncertainty conditions.

However, the PRMI exoskeleton requires tracking the wearer rapidly without obstructing. The normal sliding mode control may not solve this requirement because its asympotical convergence of system states is overcome. So, in this paper, we propose an advanced sliding mode control, called global fast terminal sliding mode control for the swing leg as shown in Fig. 5.

The dynamic equation of the 3-DOF-swing leg is written as follows:

$$T_{act} + T_{int} = M_{sw}(q_e)\ddot{q}_e + C_{sw}(q_e, \dot{q}_e)\dot{q}_e + G_{sw}(q_e). \quad (11)$$

Let the dynamic uncertainty be expressed as follows:

$$\psi(\ddot{q}_e, \dot{q}_e, q_e) = \Delta M_{sw}(q_e)\ddot{q}_e + \Delta C_{sw}(q_e, \dot{q}_e)\dot{q}_e + \Delta G_{sw}(q_e) \quad (12)$$

with $\Delta M_{sw} = M_{sw} - \hat{M}_{sw}$; $\Delta C_{sw} = C_{sw} - \hat{C}_{sw}$; $\Delta G_{sw} = G_{sw} - \hat{G}_{sw}$ and $\hat{M}_{sw}(q_e)$, $\hat{C}_{sw}(q_e, \dot{q}_e)$, $\hat{G}_{sw}(q_e)$ are the estimated values of $M_{sw}(q_e)$, $C_{sw}(q_e, \dot{q}_e)$ and $G_{sw}(q_e)$. From (11), we have:

$$\begin{aligned} T_{act} + T_{int} =& \hat{M}_{sw}(q_e)\ddot{q}_e + \hat{C}_{sw}(q_e, \dot{q}_e)\dot{q}_e + \hat{G}_{sw}(q_e) \\ &+ \psi(\ddot{q}_e, \dot{q}_e, q_e) \end{aligned} \quad (13)$$

or

$$\begin{aligned} \ddot{q}_e =& -\hat{M}_{sw}^{-1}(q_e)\left[\hat{C}_{sw}(q_e, \dot{q}_e) + \hat{G}_{sw}(q_e)\right] + \hat{M}_{sw}^{-1}(q_e)T_{act} \\ &+ \hat{M}_{sw}^{-1}(q_e)\left[T_{int} - \psi(\ddot{q}_e, \dot{q}_e, q_e)\right]. \end{aligned} \quad (14)$$

We set

$$\begin{cases} f(q_e, \dot{q}_e) = -\hat{M}_{sw}^{-1}(q_e)\left[\hat{C}_{sw}(q_e, \dot{q}_e)\dot{q}_e + \hat{G}_{sw}(q_e)\right], \\ g(q_e, \dot{q}_e) = -\hat{M}_{sw}^{-1}(q_e), \\ d(t) = \hat{M}_{sw}^{-1}(q_e)\left[T_{int} - \psi(\ddot{q}_e, \dot{q}_e, q_e)\right]. \end{cases} \quad (15)$$

Substituting (15) into (14), we have the closed-loop system as follows:

$$\ddot{q}_e = f(q_e) + g(q_e)T_{act} + d(t). \quad (16)$$

We set $x = [x_1, x_2] = [q_e, \dot{q}_e]$, x_1 and x_2 are system states. Then (16) is rewritten as follows:

$$\begin{cases} \dot{x}_1 = x_2 \\ \dot{x}_2 = f(x) + g(x)T_{act} + d(t) \end{cases} \quad (17)$$

here $f(x)$, $g(x)$ are smooth functions, $g(x) \neq 0$, $d(t)$ denotes the uncertainties and $|d(t)| \leq L$ denotes the disturbances.

Because of the advantages of fast terminal sliding mode control over normal sliding mode control as mentioned above, we select the fast sliding surface as follows:

$$s = \dot{\tilde{q}} + \alpha_0\tilde{q} + \beta_0\tilde{q}^{q_0/p_0} \quad (18)$$

with $\tilde{q} = x_1 - q_h = q_e - q_h$, q_h is human angular position (desired position command), $\alpha_0 = diag(\alpha_{01}, \alpha_{02}, \alpha_{03}) > 0$, $\beta_0 = diag(\beta_{01}, \beta_{02}, \beta_{03}) > 0$ and q_0, p_0 ($q_0 < p_0$) are positive odd numbers. $\tilde{q}^{q_0/p_0} = [\tilde{q}_1^{q_0/p_0}, \tilde{q}_2^{q_0/p_0}, \tilde{q}_3^{q_0/p_0}]^T$. The global fast sliding mode controller is designed as:

$$\begin{aligned} T_{act} =& -g(x)^{-1}\left(f(x) - \ddot{q}_h + \alpha_0\dot{\tilde{q}} + \beta_0\frac{d}{dt}\tilde{q}^{q_0/p_0} + \varnothing s\right. \\ &\left. + \gamma s^{q/p}\right), \end{aligned} \quad (19)$$

where $\gamma = diag(\gamma_1, \gamma_2, \gamma_3) > 0$, $\varnothing = diag(\varnothing_1, \varnothing_2, \varnothing_3) > 0$.

Let consider the Lyapunov function candidate as follows:

$$V = \frac{1}{2}s^T s. \quad (20)$$

Because

$$\dot{s} = \ddot{\tilde{q}} + \alpha_0\dot{\tilde{q}} + \beta_0\frac{d}{dt}\tilde{q}^{q_0/p_0} = \ddot{x}_1 - \ddot{q}_h + \alpha_0\dot{\tilde{q}} + \beta_0\frac{d}{dt}\tilde{q}^{q_0/p_0}. \quad (21)$$

Substituting (17) into (21), we get

$$\dot{s} = f(x) + g(x)T_{act} + d(t) - \ddot{q}_h + \alpha_0\dot{\tilde{q}} + \beta_0\frac{d}{dt}\tilde{q}^{q_0/p_0} \quad (22)$$

or

$$\dot{s} = -\varnothing s - \gamma s^{q/p} + d(t). \quad (23)$$

Differentiating V with respect to time in (20) we have

$$\dot{V} = s^T\dot{s} = -s^T\varnothing s - s^T\gamma s^{q/p} + s^T d(t), \quad (24)$$

where $-s^T\varnothing s \leq 0$ because $-s^T\gamma s^{q/p} + s^T d(t) \leq 0$ is satisfied, i.e., $\gamma_i \geq \left|\frac{1}{s_i^{q/p}}\right| |d_i(t)|$ or $\gamma_i \geq \left|\frac{1}{s_i^{q/p}}\right| L_i$, $i = 1, 2, 3$; therefore, we have $\dot{V} \leq 0$.

According to Lyapunov criterion, the system (11) with the control law (19) is stable when $t \to \infty$, $s \to 0$, or $\tilde{q} \to 0$. That means $q_e \to q_h$ or $T_{int} \to 0$ according to (4). This confirms that the exoskeleton is able to shadow the wearer's motions with very small interaction forces that tend to zero.

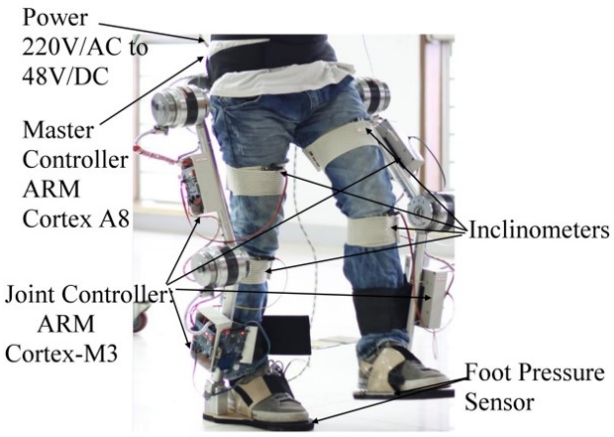

Fig. 6. The PRMI lower exoskeleton system.

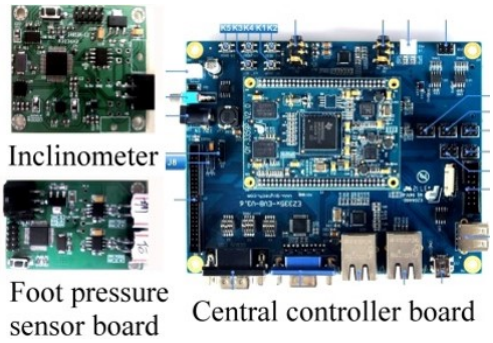

Fig. 7. Central control board and sensors.

4. THE PRMI EXOSKELETON SYSTEM

The PRMI exoskeleton is designed according to a pseudo-anthropomorphic architecture. The PRMI leg is kinematically similar to a human leg and has an adjustable mechanism for different wearers. The entire human leg has a total of 30 DOFs from the human biomechanics [22]. However, in case of exoskeleton design, it is difficult to exhibit all the DOFs of the human leg because of the complexity of such a mechanical system. For simplicity, the PRMI lower exoskeleton system is designed with typical DOFs at hip, knee and ankle joints. This design allows the PRMI exoskeleton to respond to any normal human motions during walking.

Fig. 6 describes the PRMI exoskeleton system designed for human power augmentation. Each leg in the hip structure has 2 DOFs performing functions of flexion/extension (actuated by Maxon DC motors), and abduction/adduction (non-actuated DOF). At the knee joint, there is one DOF performing flexion/extension (actuated by Maxon DC motors). There is one DOF performing dorsiflexion/planter flexion at the ankle joint and another one at the metatarsophalangeal joint for flexion/extension (non-actuated DOFs). Thus, there are only four actuated DOFs in our system using Maxon DC motors attached to a harmonic drive gear because the flexion/extension DOFs of hip and knee play an important role during normal walking and its energy consumption is also the most. The other DOFs (i.e., rotation and abduction/adduction at the ankle and rotation at the hip) are non-actuated joints controlled only by the wearer. Note that the dynamic characteristics of DOFs in the sagittal plane are investigated as mentioned in the previous section (7 DOFs in Fig. 1); the dynamic characteristics of the other DOFs in the frontal plane are ignored because of their negligible effect on system dynamics.

The sensor system consists of rotary encoders that were integrated with DC motors and located at joints to measure the angular positions of the PRMI exoskeleton system (q_e). Inclinometers were mounted on the thigh, shank and foot of the wearer via connecting bands to detect angular positions of human motions (q_h). In addition, an air pressure sensor system is located under the boot, including front and rear areas on each foot, to detect the transition of the center of gravity during walking. This helps to detect the phase transition between the two legs.

The PRMI exoskeleton system uses a power unit of 48 V/DC that was mounted on the rear of the waist structure. The master controller module of the system uses a microchip ARM Cortex-A8 and communicates with other modules via the CAN bus protocol (see Fig. 7).

5. EXPERIMENTS AND ANALYSIS

In our experiments, the wearer is a normal 25-year old male of height 175 cm and weight 61 kg. The PRMI exoskeleton system is adjusted so that it matches the wearer's body. The wearer is made to carry a load of 20 kg on his back (trunk's weight) and walk with a speed of 1.3 m/s. According to our analysis, the swing phase takes about 40% of the whole walking cycle, the stance phase takes about 60% of the whole walking cycle. The desired angular positions and velocities (q_h) are measured by the inclinometers mounted on the wearer's thigh and shank. The joint angular positions of the exoskeleton (q_e) are measured by the encoders integrated with DC motors at each joint. The role of each leg is changed from stance phase to swing phase and vice versa during walking. Air pressure sensors detecting phase transition at the bottom of the shoes monitor this process. The estimated physical parameters of the PRMI exoskeleton system are shown in Table 1. The experiments were implemented as in Fig. 8.

5.1. Stance leg

The vectors of parameter k and b can be chosen by using the forgetting factor recursive least square (FFRLS) method in [28]. k= [182,65,45,34], b= [19,13,8,4]. The experimental results are illustrated below to validate the proposed algorithm. Figs. 9 and 10 illustrate the angular

Table 1. Estimated physical parameters of the PRMI exoskeleton system - right leg (left leg).

Limbs	Mass (kg)	Length (m)	Inertial Moment (kg.m2)
Thigh	7.07 (7.12)	0.411 (0.411)	0.091 (0.093)
Shank	4.51 (4.48)	0.432 (0.432)	0.062 (0.060)
Foot	0.81 (0.803)	0.280 (0.281)	0.0105 (0.011)
Trunk	20.1	0.22	0.215

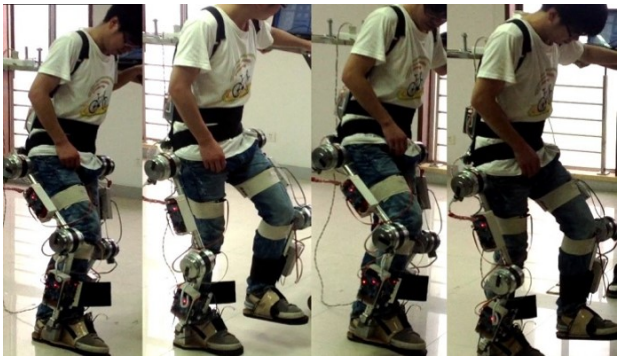

Fig. 8. Experiment of the PRMI exoskeleton system.

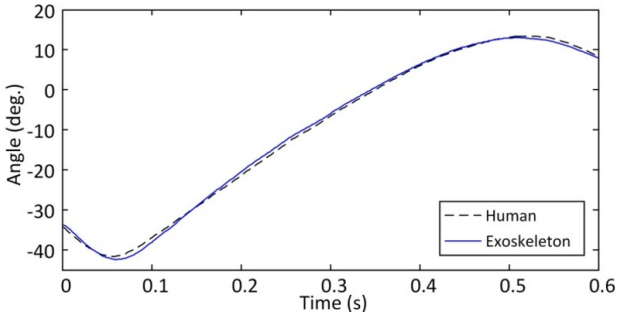

Fig. 9. Hip joint angular position tracking curves (Stance leg).

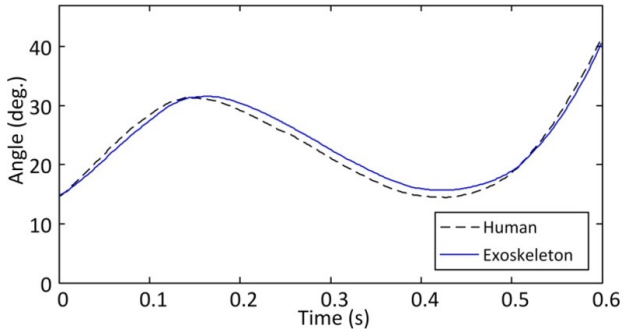

Fig. 10. Knee joint angular position tracking curves (Stance leg).

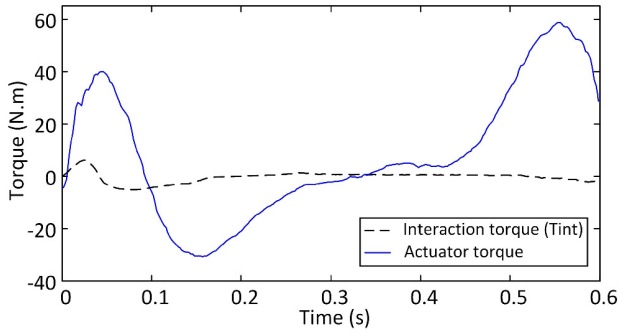

Fig. 11. Interaction and actuator torques at hip joint (Stance leg).

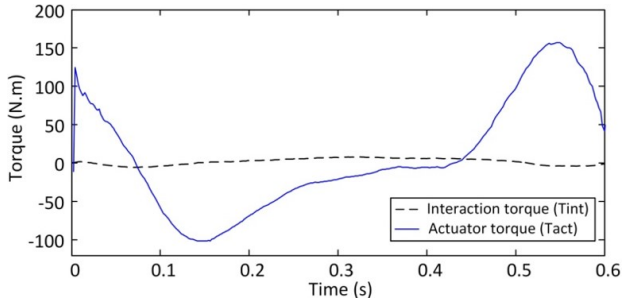

Fig. 12. Interaction and actuator torques at hip joint (Stance leg).

position tracking curves of the exoskeleton relative to the human motions at the actuated hip and knee joints in the stance phase. This phase takes about *60%* of whole walking cycle (*1s*), (the ankle joint is a non-actuated joint and imposed only by the wearer; therefore, the ankle joint is not shown in these results).

The maximum tracking error is about 2° at time points of 0.07 s and 0.56 s at the hip joint. For the knee joint, the maximum error is about 4° at time point of 0.6 s. Based on these results, we confirm that the PRMI exoskeleton is able to shadow the wearer's motions quickly with quite small interaction torques shown in Figs. 11 and 12.

The black dash-lines illustrate the interaction torques between the wearer and the exoskeleton. The blue solid-lines represent the actuator torques. According to these results, the interaction torques tend to zero while the values of the actuator torques vary from -30 to 60 Nm at the hip joint and -100 to 160 Nm at the knee joint. The values are much larger in comparison with the interaction torques. Consequently, the wearer does not feel much difference in motion while wearing the exoskeleton and walking.

5.2. Swing leg

In order to emphasize the advantage of the proposed control algorithm, we compare the proposed control algorithm with the virtual torque control algorithm [21].

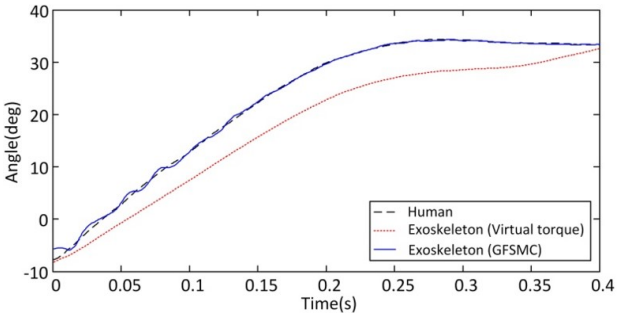

Fig. 13. Hip joint angular position tracking curves (Swing leg).

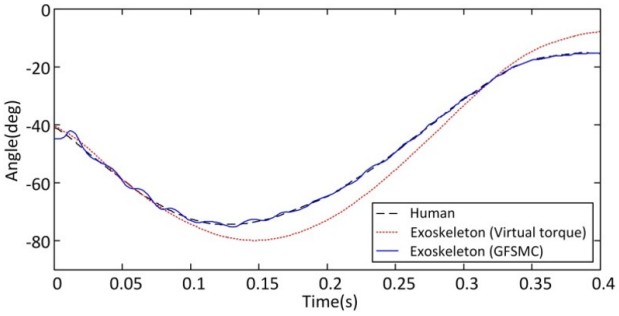

Fig. 14. Knee joint angular position tracking curves (Swing leg).

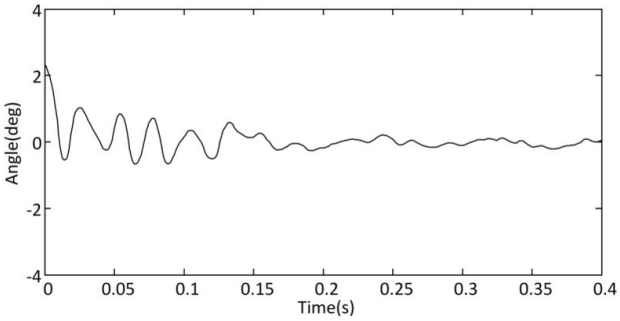

Fig. 15. Hip joint angular position error (Swing leg).

The parameters are chosen as$\varnothing = diag(4,4,3)$, $\alpha_0, = diag(4,4,3)$, $\beta_0, = diag(7,8,6)$, $q = 3$, $p = 5$, $q_0 = 3$, $p_0 = 15$. k$= [715,510,323]$, b$= [24,19,14]$. The experimental results are shown in Figs. 13-18. (The ankle joint is a non-actuated joint and imposed only by the wearer; therefore, the ankle joint is not shown in these results).

Figs. 13 and 14 show the hip and knee joint angular positions of the exoskeleton tracking relative to the wearer's motions. The results are compared with the virtual torque control algorithm in [21]. The blue solid- curves illustrate the hip and knee joint position (in degree) of the PRMI exoskeleton (q_e) that track the desired joint position of the wearer, which is illustrated by the black dash-

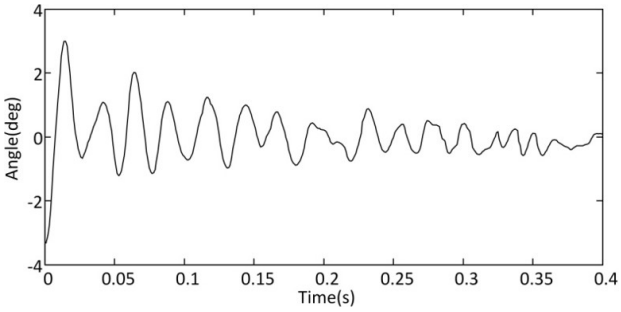

Fig. 16. Knee joint angular position error (Swing leg).

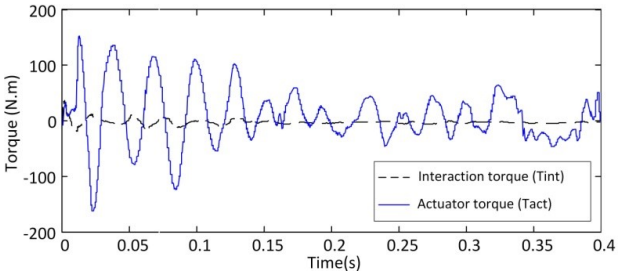

Fig. 17. Interaction and actuator torques at hip joint (Swing leg).

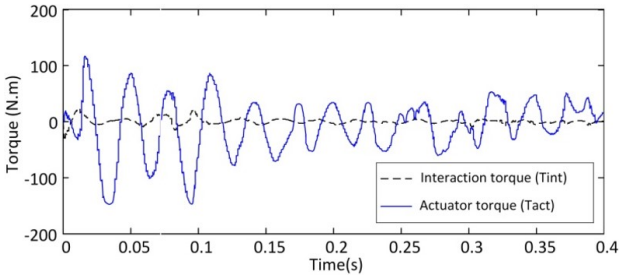

Fig. 18. Interaction and actuator torques at knee joint (Swing leg).

curves (q_h). The joint position tracking errors are maximum at the initial times of the phase (2° at the hip joint and 3° at the knee joint) and tend to zero at the end of this phase (see Figs. 15 and 16). These results confirm that the PRMI exoskeleton swing leg is able to shadow human motions in time by using the proposed controller. Meanwhile, if we use an alternative algorithm such as the virtual torque control in [21] without considering appropriate solutions to compensate the dynamic uncertainties, the hip and knee joint positions are not able to quickly shadow the wearer's motions, as illustrated by the red-dot curves in Figs. 13, and 14. Figs. 17 and 18 show the correlation between the generated actuator torques (T_{act}– blue-solid curves) and interaction torque imposed by the wearer (T_{int} – black-dash curves). The generated actuator torques (T_{act}) are much larger in comparison with the interaction torques imposed by the wearer (T_{int}). The generated actuator torques are quite large and vary from *-160* to

+150 Nm and *-150* to *+120 Nm* at the hip and knee joint, respectively. Meanwhile, the interaction torques imposing on the wearer (black-dash lines) are quite small (the maximum values are *-15* to *+30 Nm* and *-30* to *+20 mm* at the hip and knee joint, respectively) and tend to zero at the end of the swing phase. These results show that the generated actuator torques play a key role to support heavy carrying during walking, and the very small interaction forces make the wearer swing comfortably during walking.

6. CONCLUSION AND FUTURE WORK

This paper has presented a hybrid control algorithm by using the PD controller with gravity compensation and the global fast sliding mode controller for each leg of the exoskeleton. Our results show that the PRMI exoskeleton has a great ability to enhance human performance during walking. Indeed, we have reduced the complexity of the system by focusing on controlling the stance leg and the swing leg separately. The proposed controller also allows eliminating the complicated force sensors that were earlier installed at the human-exoskeleton interaction positions . Remarkably, the robustness of the system has improved significantly because the proposed controller is capable of stabilizing the system against the unknown uncertainties. We have validated the proposed control algorithm with the PRMI exoskeleton system built by the University of Electronic Science and Technology of China. Our experimental results also show that the exoskeleton system plays a key role in human power augmentation by tracking the motion and performances of the wearer quickly while keeping the human-exoskeleton interaction forces really small. This achievement can be related to the future work that will be focused on cognitive human robot interaction to enhance the performance of the robot.

REFERENCES

[1] W. Huo, S. Mohammed, J. C. Monero, and Y. Amirat, "Lower limb wearable robots for assistance and rehabilitation: a state of the art," *IEEE Systems Journal*, no. 99, pp. 1-14, 2015. [click]

[2] C. Mendez, Y. Aoustin, and C. Rengifo, "Evaluation of the aid provided by an exoskeleton in the reduction of the joint torques exerted by human lower limbs: a simulation study," *Latin America Transactions, IEEE (Revista IEEE America Latina)*, vol. 13, no. 2, pp. 428-433, 2015. [click]

[3] D. Chen, M. Ning, B. Zhang, and G. Yang, "Control strategy of the lower-limb exoskeleton based on the EMG signal," *Proc. of IEEE International Conference on Robotics and Biominmetrics (ROBIO)*, pp. 2416-2420, 2014. [click]

[4] A. C. Christine and V. K. Herman, "Assistive and rehabilitation robotics," *Journal of Behavioral Robotics*, vol. 2, no. 4, pp. 175-185, 2011. [click]

[5] X. Zhang, Z. Xiang, Q. Lin, and Q. Zhou, "The design and development of a lower limbs rehabilitation exoskeleton suit," *Proc. of International Conference on Complex Medical Engineering (CME)*, pp. 307-312, 2013. [click]

[6] Z. Li, C. Y. Su, and A. Xue, "Development and learning control of a human limb with a rehabilitation exoskeleton," *IEEE Transactions on Industrial Electronics*, vol. 61, no. 7, pp. 3776 - 3785, 2014. [click]

[7] E. Rocon and J. L. Pons, *Exoskeletons in Rehabilitation Robotics*, Springer, Berlin Heidelberg, 2011. [click]

[8] C. T. Freeman, D. Tong, Z. Cai, E. Rogers, K. Meadmore, and A. M. Hugers, "Phase-lead iterative learning control algorithms for functional electrical stimulation-based stroke rehabilitation," *Proc IMechE, Part I: J Systems and Control Engineering*, vol. 225, no. 6, pp. 850-859, 2011. [click]

[9] A. Tsukahara, Y. Hasegawa, and Y. Sankai, "Gait support for complete spinal cord injury patient by synchronized leg-swing with HAL," *Proc. of IROS*, pp. 1737-1742, 2011. [click]

[10] F. Veneman, R. Kruidhof, and H. V. D. Kooij, "Design and evaluation of the LOPES exoskeleton robot for interactive gait rehabilitation," *IEEE TNSRE*, vol. 15, no. 3, pp. 379-386, 2007. [click]

[11] A. M. Sander, "Rehabilitation: a demonstration of the art and science," *Robotica,* vol. 7, pp. 533-534, 2001. [click]

[12] H. Kim, J. Lee, J. Jang, S. Park, and C. Hang, "Design of an Exoskeleton with Minimized Energy Consumption based on using Elastic and Dissipative Elements," *International Journal of Control, Automation and Systems*, vol. 13, no. 2 , pp. 1-12, 2015. [click]

[13] H. Kazerooni, "Human-Robot Interaction via the Transfer of Power and Information Signals," *IEEE TSMC*, vol. 20, no. 2, pp. 450-463, 1990. [click]

[14] H. Kazerooni and S. Mahoney, "Dynamics and Control of Robotic Systems Worn By Humans," *ASME Journal of Dynamic Systems, Measurements, and Control*, vol. 113, no. 3, pp. 379-387, 1991. [click]

[15] H. Kazerooni and M. Her, "The Dynamics and control of a haptic interface device," *IEEE Trans. on* Robotics and Automation, vol. 10, no. 4, pp. 453-464, 1994. [click]

[16] H. Kazerooni, "The extender technology at the University of California, Berkeley," *Proc. of SICE*, vol. 34, pp. 291-298, 1995.

[17] H. Kazerooni, "Human augmentation and exoskeleton systems in Berkeley," *IJHR*, vol. 4, no. 3, pp. 575-605, 2007. [click]

[18] H. Kazerooni, "Exoskeleton for human power augmentation," *Proc. of IEEE/RSJ IROS*, pp. 3459-3464, 2005. [click]

[19] A. Zoss, H. Kazerooni, and A. Chu, "On the mechanical design of the Berkeley Lower Extremity Exoskeleton (BLEEX)," *IEEE/RSJ IROS*, pp. 3465-3472, 2005. [click]

[20] H. Kazerooni, J. L. Racine, L. Huang, and R. Steger, "On the control of the Berkeley Lower Extremity Exoskeleton (BLEEX)," *IEEE ICRA*, pp. 4353-4360, 2005. [click]

[21] H. Kazerooni, R. Steger, and L. Huang, "Hybrid control of the Berkeley Lower Extremity Exoskeleton (BLEEX)," *IJRR Journal*, vol. 25, no. 5-6, pp. 561-573, 2006. [click]

[22] Z. Yang, L. Gui, X. Yang, and W. Gu, "Simulation research of exoskeleton suit based on neural network sensitivity amplification control," *IEEE ICAL*, pp. 3340-3344, 2007. [click]

[23] Z. Yang, Y. Zhu, X. Yang, and Y. Zhang, "Impedance control of exoskeleton suit based on RBF adaptive network," *International Conference on Intelligent Human-Machine Systems and Cybernetics*, pp. 182-187, 2009. [click]

[24] K. H. Low, X. Liu, and H. Yu, "Development of NTU wearable exoskeleton system for assistive technologies," *Proc. of IEEE International Conference on Mechatronics and Automation*, pp. 1099-1105, 2005. [click]

[25] Y. Sankai, "HAL: Hybrid assistive limb based on cybernics," *Springer Tracts in Advanced Robotics*, vol. 66, pp. 25-34, 2011. [click]

[26] J. Liu and X. Wang, *Advanced Sliding Mode Control for Mechanical Systems*, Tsinghua University Press, Beijing and Springer-Verlag Berlin Heidelberg, 2011. [click]

[27] V. Utkin, J. Guldner, and J. Shi, *Sliding Mode Control in Electromechanical Systems*, Taylor & Francis, London, 1999.

[28] Q. Bi, C. J. Yang, X. L. Deng, and J. C. Fan, "Human finger mechanical impedance modeling: Using multiplicative uncertain model," *Proceedings of the Institution of Mechanical Engineers, Part C: Journal of Mechanical Engineering Science*, pp. 1-9, 2015. [click]

Duong Mien Ka is a Ph.D. research student at University of Electronic Science and Technology of China. Now, he is also a lecturer at Faculty of Electronic Technology, Industrial University of Ho Chi Minh City, Viet Nam. He received the M.S. degree in Automation from Ho Chi Minh City University of Technology in 2010. His current research interests include mechatronics systems, intelligent robotic control, and human power augmentation exoskeleton.

Cheng Hong is a full Professor in School of Automation, a vice director of Center for Robotics, UESTC. He received Ph.D. degree in Pattern Recognition and Intelligent Systems from Xi'an Jiaotong University in 2003. Now he is the founding director of Pattern Recognition and Machine Intelligence Lab, UESTC. Before this, He was a postdoctoral at Computer Science School, Carnegie Mellon University, USA from 2006 to 2009. He was an associate Professor of Xi'an Jiaotong University since 2005. Since July 2000, he had been with Xi'an Jiaotong University, where he had been a team leader of intelligent Vehicle Group at the Institute of Artificial Intelligence and Robotics before going to USA. His current research interests include computer vision and machine learning, robotics, human computer interaction, multimedia signal processing. The team that Dr. Cheng was leading in XJTU had developed an intelligent driving platform-Spring robot, which has important social effect in China. Dr. Cheng has over 50 academic publications including two books-"Digital Signal Processing (Tsinghua University Press, Sep. 2007)" and "Autonomous Intelligent Vehicles: Theory, Algorithms and Implementation (Springer, Dec. 2011)". He has been a senior member of IEEE, ACM, and Associate Editor of IEEE Computational Intelligence Magazine. He is a reviewer for many important journals and conferences (IEEE TITS, MAV, CVPR, ICCV, ITSC, IVS, ACCV, etc.). Dr. Cheng serves as Finance Chair of ICME 2014, Local arrangement chair of VLPR 2012, Registration Chair of the 2005 IEEE ICVES Dr. Cheng was teaching Digital Signal Processing and Introduction to Embedded systems for junior students at Automation department and also Advanced Digital Signal Processing for graduate students in Xi'an Jiaotong University. Now he is teaching Pattern Recognition and Machine Learning and Computer Vision for graduate students, and also Introduction to Artificial Intelligence and Digital Image Processing for junior students in UESTC.

Tran Huu Toan received the M.S. degree in Automation from Ho Chi Minh City University of Technology in 2009, and the Ph.D degree in Electronic Science and Technology from University of Electronic Science and Technology of China in 2015. His research interests include control applications, robot learning, and human-robot interaction.

Jing Qiu is currently working in the School of Mechatronics Engineering at the University of Electronic Science and Technology of China (UESTC). Prior to joining UESTC, she was a research assistant at the Institute of Ergonomics at Darmstadt University of Technology. She received her Ph.D. in ergonomics from Darmstadt University of Technology in 2010.